Vehicle System Dynamics
Vol. 00, No. 00, Month 200x, 1–17

Preprint of final paper. © 2008 Taylor & Francis DOI: 10.1080/00423110701790723

Stability control of 4WS vehicles using robust IMC techniques[†]

M. Canale [‡§] and L. Fagiano[§]

(*Received 00 Month 200x; In final form 00 Month 200x*)

A robust non parametric approach to vehicle stability control by means of a four wheel steer by wire system is introduced. Both yaw rate and sideslip angle feedbacks are used in order to take into account effectively safety as well as handling performances. Reference courses for yaw rate and sideslip angle are computed on the basis of the vehicle speed and of the handwheel angle imposed by the driver. An output multiplicative model set is used to describe the uncertainty arising from the wide range of the vehicle operating situations. The effects of saturation of the control variables (i.e. front and rear steering angles) are taken into account by adopting enhanced Internal Model Control methodologies in the design of the feedback controller. Actuator dynamics are considered in the controller design. Improvements on understeer characteristics, stability in demanding conditions such as turning on low friction surfaces, damping properties in impulsive maneuvers and improved handling in closed loop (i.e. with driver feedback) maneuvers are shown through extensive simulation results performed on an accurate 14 degrees of freedom nonlinear model, which proved to give good modeling results as compared to collected experimental data.

1 Introduction

Vehicle active control systems aim to enhance handling and comfort characteristics ensuring stability in critical manoeuvering situations. A commonly employed solution is made up by the use of a yaw rate feedback realized by means of suitable yaw moments (as control inputs) that can be generated in different ways. In particular, the action of active braking systems is employed in Anti-lock Braking System (ABS), Vehicle Dynamic Control (VDC) and Electronic Stability Program (ESP) strategies; an electronic controlled superposition of an angle to the steering wheel is used in Front Active Steering methodologies; unsymmetrical force distributions for left-right sides of the axles are imposed by means of active differential devices; rear steering angle input is applied in Four Wheel Steering systems (see [1] and the references therein for an extensive summary). As a matter of fact, in emergency situations like braking or turning on low friction surfaces it is needed to avoid too large values of the sideslip angle to enhance vehicle safety (see [2]). Besides, sideslip angle has to be limited to low values (e.g. $\pm 4^\circ$) to improve the stability feelings perceived by the driver. Therefore, improvements on the overall performances can be achieved if a sideslip angle feedback is employed in addition to the yaw rate loop.
In this paper, the problem of vehicle stability control is considered for a vehicle equipped with a four wheel steer by wire system. Several solutions have been introduced in the last years in the context of four wheel steering (4WS) systems. In particular, in [3], the rear steering angle is commanded on the basis of the front steering angle, in [4] a feedback-feedforward structure is employed to control the rear steering angle while the front steering angle remains under the driver control. More specifically, the use of 4WS by wire has been considered e.g. in [5], where the proposed control structure is able to decouple the control of lateral acceleration and the yaw rate control, and in [6], where Individual Channel Design techniques have been used to design yaw rate and sideslip angle feedbacks. A common problem to all 4WS solutions is the fact that the values of both the front and rear steering angles are subject to physical constraints causing the saturation of the input variables with possible deteriorations of the control performances. An analysis of the saturation effects on the stability performances has been introduced in [6]. In addition, as the vehicle operates under a wide range of conditions of speed, load, friction etc., the active control system has to guarantee safety (i.e. stability) performances robustly in face of the uncertainty arising from such operating situations. Robustness of active vehicle systems is a widely studied topic and interesting results have recently appeared using parametric and non parametric approaches (see e.g. [7], [8], [9], [10] and [11]).

[†]This research was partly supported by funds of Ministero dell'Università e della Ricerca under the Projects "Advanced control and identification techniques for innovative applications" and "Control of advanced systems of transmission, suspension, steering and braking for the management of the vehicle dynamics".

[‡]Corresponding author. Email: massimo.canale@polito.it Tel.:+39-011-0907063

[§]The authors are with Dipartimento di Automatica e Informatica, Politecnico di Torino, Corso Duca degli Abruzzi 24 - 10129 Torino - Italy

Vehicle System Dynamics
ISSN 0042-3114 print / ISSN 1744-5159 online © 200x Taylor & Francis
http://www.tandf.co.uk/journals
DOI: 10.1080/0042311YYxxxxxxx

Therefore, the designer of the control system has to take care of both robust stability and control saturation aspects. As to the choice of the control structure to be adopted a yaw rate plus sideslip angle multivariable feedback has been considered. Internal Model Control (IMC) techniques are used in the design of the controller as they are well established control methodologies able to handle in an effective way both robustness (see [12]) and saturation (see e.g. [13]) issues. In particular, the enhanced IMC structure presented in [14], which guarantees robust stability as well as improved performances in presence of saturation of the control inputs, will be employed. As such design methodology is based on robust H_∞ optimization techniques, a linear model of the lateral vehicle dynamics will be considered and an unstructured uncertainty description approach will be adopted to take into account the different operating conditions of the vehicle. **Moreover, IMC methodology has proved to be an effective tool in vehicle stability control. In fact, in [11] such approach has been successfully employed in a feedforward-feedback structure, in yaw control context with an active differential device.** In order to show in a realistic way the effectiveness of the proposed control approach, simulations will be performed using a detailed nonlinear 14 degrees of freedom vehicle model of an Alfa Romeo segment E prototype car, which proved to give an accurate description of the vehicle dynamics as compared with actual vehicle measurements. Actuator dynamics effects have been included too. The objective of this paper is to show the potentiality of the proposed approach which takes robustly into account both stability and saturation effects. It is assumed that both yaw rate and sideslip angle are measured. However, it is a well known fact that the estimation of sideslip angle is a critical issue. On the other hand, quite good and accurate solutions have been proposed in the literature (see e.g. [2], [15] and [16]) ensuring the reliability of suitable control techniques involving sideslip angle loops. The paper is organized as follows. In Section 2 problem settings and control requirements will be introduced. Vehicle modeling issues are presented in Section 3 while the adopted control structure and the related design principles are described in Section 4. Finally, in Section 5, extensive simulation studies are reported in order to show the effectiveness of the proposed approach under a wide range of driving scenarios.

2 Problem formulation

Vehicle stability control aims to change steady state and transient behaviour of the car, enhancing handling performances in turning maneuvers and keeping safety in presence of unusual external conditions and/or critical maneuvers, such as handwheel steps needed to avoid obstacles, braking under different left-right side adhesion conditions and lateral wind forces. The considered vehicle is equipped with a four wheel steer by wire system, thus the control inputs are the front and rear steering actuators commands, δ_f^i and δ_r^i respectively. The actuators impose the front and rear steering angles, δ_f and δ_r. Therefore, the handwheel angle δ issued by the driver is not directly transmitted to the wheels but it is used to describe her/his driving intention in the reference generation design as it will be explained in Section 4. The controlled variables are vehicle yaw rate $\dot{\psi}(t)$ and sideslip angle $\beta(t)$ as they allow to take into account vehicle safety and handling requirements as well as improvements of the driver stability feeling (see [1]). To define the vehicle steady state (i.e. constant speed) requirements in turning maneuvers we recall that, as a first approximation, considering car and suspension system as a rigid body moving at constant speed v, the following relationship links $\dot{\psi}(t)$ and $\dot{\beta}(t)$ to the lateral acceleration $a_y(t)$ (see e.g. [1]):

$$a_y(t) = v(\dot{\psi}(t) + \dot{\beta}(t))$$

In steady state motion vehicle sideslip angle is constant and lateral acceleration is therefore proportional to the yaw rate through the vehicle speed. For each constant speed value, by means of standard steering pad maneuvers it is possible to obtain the steady state lateral acceleration (and yaw rate) corresponding to different values of the handwheel angle. These values can be graphically represented on the vehicle *steering diagram* (Figure 1.(a)), where the handwheel angle is reported with respect to the lateral acceleration (see [17] and the references therein). Such curves are mostly influenced by road friction and depend on the tyre lateral force-slip characteristics. The curve course may be divided into two tracts: at low acceleration the shape is linear and its slope is a measure of the readiness of the car, since the lower this value, the higher the lateral acceleration reached by the vehicle with the same handwheel angle, the more the sport feeling and handling quality perceived by the driver (see e.g. [18]). At high acceleration values the curve course becomes nonlinear showing a saturation value for a_y, that is the highest lateral acceleration the vehicle can reach. The intervention of an active device able to change left/right longitudinal

tyre forces distribution or wheel steering angles can be employed to vary, given the same speed and handwheel angle conditions, the behaviour of a_y, modifying the steering diagram slope according to some desired requirements. The enhancements obtained by such vehicle stability systems can be described by means of an improved steering diagram (as shown in Figure 1.(a), solid line), which can be considered as a target performance to be obtained by the control system. More details about the definition of target steering diagrams will be given in Section 4.1. In particular, it will be shown how appropriate yaw rate references can be generated on the basis of the desired understeer performances. As regards the desired sideslip angle behaviour a similar approach could be followed

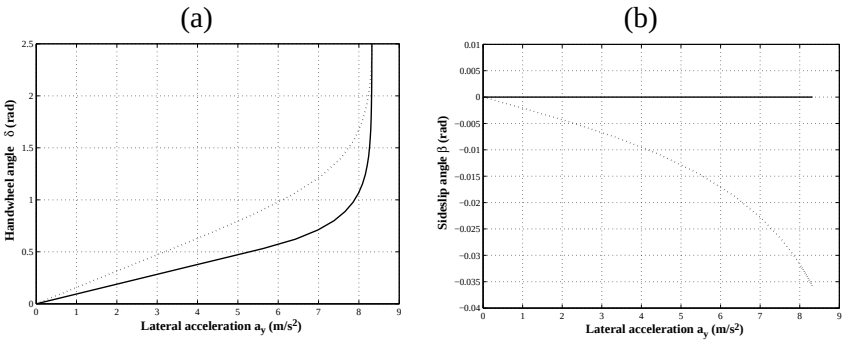

Figure 1. Uncontrolled vehicle (dotted lines) and target (solid lines) (a) steering diagram and (b) sideslip angle curve. Vehicle speed $v = 100$ km/h

using sideslip curves (i.e. β vs. a_y) as depicted in Figure 1.(b). In particular, as the smaller is the slide-slip angle the more comfortable are the turning maneuvers, the aim is to keep β value as low as possible (namely zero). The design of a suitable sideslip reference is described in Section 4. Therefore improvements on the understeer and sideslip performances may be obtained using suitable modifications of the vehicle lateral dynamics in steady state conditions. A reference generator will provide the values for the controlled variables needed to achieve the desired performances by means of the feedback controller. As a matter of fact, also in critical maneuvering situations such as fast path changing at high speed or braking and steering with low and non uniform road friction vehicle dynamics need to be improved in order to enhance stability and handling performances. In particular, given the swiftness of such maneuvers the transient vehicle response needs to satisfy good damping and readiness properties. This can be taken into account in the control design imposing suitable closed loop bandwidth and well damped characteristics. Needless to say that at least safety (i.e. stability) requirements have to be guaranteed in face of the uncertainty arising from the wide range of the vehicle operating conditions of speed, load, tyre, friction etc.. This can be achieved by means of a robust design using an appropriate description of the uncertainty as it will be described in the following Sections 3 and 4. Moreover, to take into account the effects of saturation of the steering angles (i.e. the maximum allowed values for δ_f^i and δ_r^i), the control structure should be provided by suitable implementation solutions like anti-windup schemes to avoid performance degradation in such occurrences.

3 Model description

The standard single track vehicle model, **depicted in Figure 2 for a 4WS vehicle**, has been used to describe the vehicle dynamics (see e.g. [1]). **In particular, in Figure 2, vehicle yaw rate ψ, sideslip angle β and steering angles δ_f and δ_r are showed, as well as the vehicle speed v and the velocities at the front and rear wheels, v_f and v_r respectively. The front and rear slip angles, α_f and α_r, are reported too. The wheelbase is indicated with l, while a and b are the distances between the center of gravity (C.O.G.) and the front and rear axles respectively**.

The employed model is based on the following **standard** (see e.g. [1]) assumptions:

- Flat road.
- Longitudinal motion resistances are ignored compared to wheel lateral forces.
- Self aligning wheel moments are ignored.
- Front and rear steering angles and vehicle sideslip angle are small enough to linearize their trigonometrical functions.
- Vehicle speed is a known parameter, vehicle longitudinal acceleration is low or equal to zero.

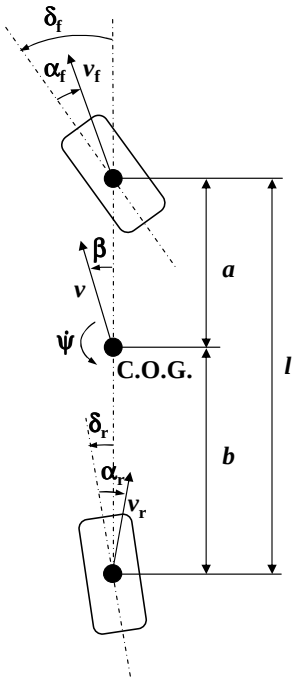

Figure 2. Single track schematic.

According to the standard maneuvering test set considered in this paper (see Section 5), steering and sideslip angles are limited to quite small values, thus rendering well-funded the assumptions made. Moreover, δ_r is small even when the related control input saturates.
Dynamic generation of tyre forces has been modelled too by means of tyre lateral relaxation lengths, giving rise to the following equations:

$$\begin{aligned} &mv(t)\dot{\beta}(t) + mv(t)\dot{\psi}(t) = F_{yf,p}(t) + F_{yr,p}(t) \\ &J_z\ddot{\psi}(t) = aF_{yf,p}(t) - bF_{yr,p}(t) \\ &F_{yf,p}(t) + l_f/v\dot{F}_{yf,p}(t) = -c_f(\beta(t) + a\dot{\psi}(t)/v(t) - \delta_f(t)) \\ &F_{yr,p}(t) + l_r/v\dot{F}_{yr,p}(t) = -c_r(\beta(t) - b\dot{\psi}(t)/v(t)) - \delta_r(t)) \end{aligned} \tag{1}$$

where m is the vehicle mass and J_z is the moment of inertia around the vertical axis; the front and rear tyre relaxation lengths are indicated as l_f and l_r, while the symbols c_f and c_r stand for the front and rear axle cornering stiffnesses. $F_{yf,p}$ and $F_{yr,p}$ are the front and rear axle lateral forces.
Using equations (1), the vehicle dynamics can be described for a fixed value v of its speed by the following transfer matrix $G^{\delta}_{f,r}(s)$ in the Laplace domain:

$$\begin{bmatrix} \dot{\psi}(s) \\ \beta(s) \end{bmatrix} = \underbrace{\begin{bmatrix} G_{\delta_f,\dot{\psi}}(s) & G_{\delta_r,\dot{\psi}}(s) \\ G_{\delta_f,\beta}(s) & G_{\delta_r,\beta}(s) \end{bmatrix}}_{G^{\delta}_{f,r}(s)} \begin{bmatrix} \delta_f(s) \\ \delta_r(s) \end{bmatrix} \tag{2}$$

with

$$G_{\delta_f,\dot{\psi}}(s) = \frac{b_2s^2 + b_1s + b_0}{a_4s^4 + a_3s^3 + a_2s^2 + a_1s + a_0} \quad G_{\delta_r,\dot{\psi}}(s) = \frac{c_2s^2 + c_1s + c_0}{a_4s^4 + a_3s^3 + a_2s^2 + a_1s + a_0}$$
$$G_{\delta_f,\beta}(s) = \frac{d_2s^2 + d_1s + d_0}{a_4s^4 + a_3s^3 + a_2s^2 + a_1s + a_0} \quad G_{\delta_r,\beta}(s) = \frac{e_2s^2 + e_1s + e_0}{a_4s^4 + a_3s^3 + a_2s^2 + a_1s + a_0}$$

and

$$
\begin{aligned}
&a_4 = mJ_z l_f l_r,\ a_3 = mvJ_z(l_f + l_r),\ a_2 = J_z(mv^2 + c_f l_r + c_r l_f) + m(c_f a^2 l_r + c_r b^2 l_f)\\
&a_1 = v(J_z(c_f + c_r) + m(c_f a(a - l_r) + c_r b(b + l_f))),\ a_0 = c_f c_r l^2 - mv^2(c_f a - c_r b)\\
&b_2 = mvac_f l_r,\ b_1 = mv^2 ac_f,\ b_0 = vc_f c_r l\\
&c_2 = -mvbc_r l_f,\ c_1 = -mv^2 bc_r,\ c_0 = -vc_f c_r l\\
&d_2 = c_f J_z l_r,\ d_1 = vc_f(J_z - mal_r),\ d_0 = c_f c_r bl - mv^2 ac_f\\
&e_2 = c_r J_z l_f,\ e_1 = vc_r(J_z + mbl_f),\ e_0 = c_f c_r al + mv^2 bc_r
\end{aligned}
$$

Actuator dynamics are modelled as second order systems with delay (see [19]):

$$
\begin{bmatrix} \delta_f(s) \\ \delta_r(s) \end{bmatrix} = \underbrace{\begin{bmatrix} G_{a,f}(s) & 0 \\ 0 & G_{a,r}(s) \end{bmatrix}}_{G_a{}'(s)} e^{-\vartheta s} \begin{bmatrix} \delta_f^i(s) \\ \delta_r^i(s) \end{bmatrix} = G_a(s) \begin{bmatrix} \delta_f^i(s) \\ \delta_r^i(s) \end{bmatrix} \tag{3}
$$

with

$$
\begin{aligned}
G_{a,f}(s) &= K_f \frac{\omega_f^2}{s^2 + 2\zeta_f \omega_f s + \omega_f^2}\\
G_{a,r}(s) &= K_r \frac{\omega_r^2}{s^2 + 2\zeta_r \omega_r s + \omega_r^2}
\end{aligned} \tag{4}
$$

Where δ_f^i and δ_r^i are the inputs to the front and rear steering actuators respectively (i.e. the controller outputs), K_f, K_r are the front and rear actuator gains, ζ_f, ζ_r are the damping ratios and ω_f, ω_r the natural frequencies. ϑ is the considered transmission delay, which is equal for the front and rear actuators (as it is assumed in [19]).
Thus, the following nominal model will be considered in the controller design:

$$
G_{Plant} = G(s)\, e^{-\vartheta s} \tag{5}
$$

where $G(s) = G_{f,r}^{\delta}(s) G_a{}'(s)$ (see (2) and (3)). Model (5) is computed according to a nominal operating condition defined by the related values of the vehicle and actuator parameters. As already remarked, the real vehicle behaviour is influenced by several different factors that introduce model uncertainty. Therefore, in order to perform a robust design, an output multiplicative model set of the form (6) has been employed in the control design:

$$
\mathcal{G}(G, \Gamma) = \{(I + \Delta(s))G(s) : \bar{\sigma}(\Delta(j\omega)) \leq \Gamma(\omega)\} \tag{6}
$$

A scheme of model set (6) is reported in Figure 3. Such model set has been obtained taking into account the effects of different vehicle speeds ($\pm$ 20% of the nominal value), inertial characteristics ($\pm$ 10% of the nominal mass with consequent geometrical parameters changes) cornering stiffnesses ($\pm$ 5% of the nominal values) and tyre relaxation lengths ($\pm$ 5% of the nominal values). The course of the frequency behaviour of the maximum singular

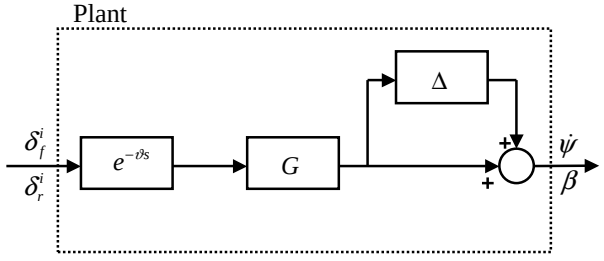

Figure 3. Plant model scheme

value $\bar{\sigma}(\Delta(\omega))$ is obtained by gridding on the considered model parameter variations (see [20]) and is reported in

Figure 9 of Section 5 .
Finally, to compute the reference values for yaw rate and sideslip angle, a single track nonlinear static model is also considered in this paper. Such a model is described in [11] and accounts for the nonlinear axle slip-lateral force relationship introduced in [21]:

$$F_{y,p}(\alpha) = D(C\arctan(B(-\alpha+S_h) - E(B(-\alpha+S_h) - \arctan(B(-\alpha+S_h))))) + S_v \tag{7}$$

where α is the axle slip angle. B, C, D, E, S_h, S_v are parameters which can be identified using the experimental data collected during standard handling maneuvers. In the considered settings, front and rear slip angles **(see Figure 2)** can be written as:

$$\begin{aligned} \alpha_f &= \beta + a\dot{\psi}/v - K_f\delta_f^i \\ \alpha_r &= \beta - b\dot{\psi}/v - K_r\delta_r^i \end{aligned} \tag{8}$$

thus, front and rear axle lateral forces can be expressed as nonlinear functions of β, $\dot{\psi}$, δ_f^i, δ_r^i. Moreover, in steady state conditions (i.e. $\ddot{\psi} = 0,\ \dot{\beta} = 0$) the first two equations of (1) can be rewritten as

$$\begin{aligned} mv\dot{\psi} &= F_{yf,p} + F_{yr,p} \\ aF_{yf,p} - bF_{yr,p} &= 0 \end{aligned} \tag{9}$$

then, by replacing $F_{yf,p}$ and $F_{yr,p}$ in (9) with the corresponding expressions obtained from equation (7), the single track steady state nonlinear model equations can be obtained as:

$$\begin{aligned} mv\dot{\psi} &= F_{yf,p}(\beta,\dot{\psi},\delta_f^i) + F_{yr,p}(\beta,\dot{\psi},\delta_r^i) \\ aF_{yf,p}(\beta,\dot{\psi},\delta_f^i) &- bF_{yr,p}(\beta,\dot{\psi},\delta_r^i) = 0 \end{aligned} \tag{10}$$

The solution of such equations for given values of the variables δ_f^i, δ_r^i provides any feasible steady state motion condition (i.e. β and $\dot{\psi}$) for the nominal vehicle.

4 IMC approach to yaw control

The employed control structure is depicted in Figure 4. The desired yaw rate and sideslip angle reference signals

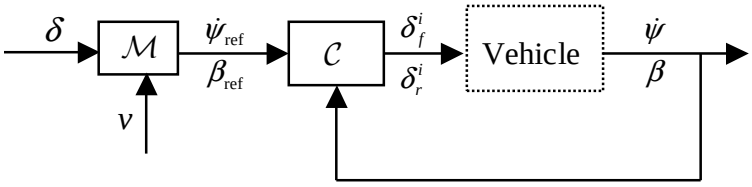

Figure 4. Considered control structure.

$\dot{\psi}_{\text{ref}}(t)$, $\beta_{\text{ref}}(t)$ are generated by a static map $\mathcal{M}$ using the instantaneous values of $\delta(t)$ and $v(t)$. The feedback controller $\mathcal{C}$ computes the inputs for the front and rear steering actuators, $\delta_f^i(t)$ and $\delta_r^i(t)$, needed to obtain the required performances described by $\dot{\psi}_{\text{ref}}(t)$ and $\beta_{\text{ref}}(t)$.

4.1 *Reference generator*

Reference yaw rate and sideslip angle values are generated using a nonlinear static map

$$\begin{bmatrix} \dot{\psi}_{\text{ref}} \\ \beta_{\text{ref}} \end{bmatrix} = \mathcal{M}(\delta, v) \tag{11}$$

which uses as inputs the handwheel angle δ imposed by the driver and the vehicle speed v. The map $\mathcal{M}(\delta, v)$ is generated according to the control objective, i.e. to keep small sideslip angle values while improving the vehicle manoeuvrability, thus enhancing the overall vehicle handling quality perceived by the driver (see [18]). To compute the map values, the single track nonlinear steady state vehicle model (10) is employed in a three-step procedure. First of all, equations (10) are solved considering any combination of control inputs inside the actuator limitations to compute all the possible controlled vehicle motion conditions within the vehicle lateral acceleration limit. Thus, for each constant speed value, the working region in the plane (a_y, δ) is obtained (see Figure 5.(a), solid lines). This region represents a limit to the reference steering diagram that can be set for the controlled vehicle with the nominal tyre, mass and geometrical characteristics. In the second step, reference yaw rate values $\dot{\psi}_{\text{ref}}(\delta, v)$ are

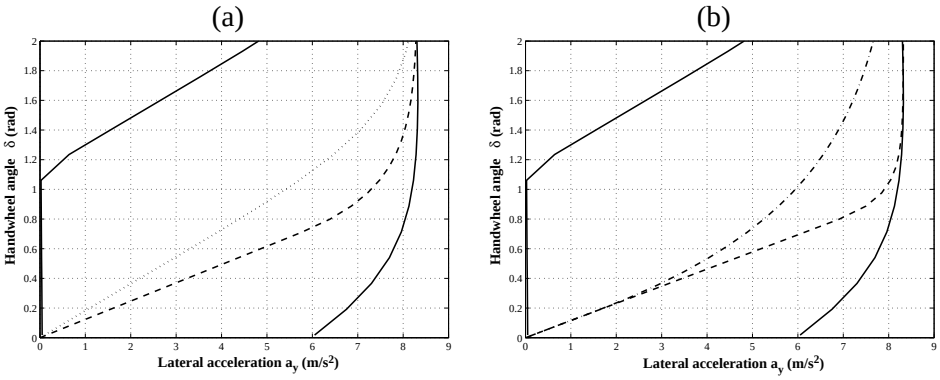

Figure 5. (a) Control system working region, delimited by solid lines, and uncontrolled (dotted) and reference (dashed) vehicle steering diagrams. (b) Different possible reference steering diagram choices for the nonlinear tract. Speed: 80 km/h

obtained by choosing, at each speed value, the reference steering diagram within the working region, according to some performance criteria (e.g. to improve the vehicle manoeuvrability by reducing the slope of the curve for small values of lateral acceleration). To this end, the steering diagram can be divided into a linear tract (at small lateral acceleration values) and into a nonlinear one. In the first tract, a commonly employed performance criterium is to improve the vehicle maneuverability by reducing the slope of the curve. In the nonlinear tract, a trade off has to be chosen: on the one hand, it is suitable to modify the nonlinear part of the curve in order to increase the lateral acceleration range for which the controlled vehicle understeer characteristic behaves linearly (see e.g. Figure 5.(b), dashed line); on the other hand, it is also needed a smooth connection of the linear tract with the maximum lateral acceleration value (as reported in Figure 5.(b), dash-dotted line), to avoid the driver to suddenly feel that the car has reached its cornering limit, after which a steering angle increment does not correspond to a lateral acceleration increment (i.e. the cornering radius cannot be shortened by means of a simple steering action), thus likely giving place to critical driving situations. From a practical point of view, the two steering diagrams reported in Figure 5.(b) can be associated to different vehicle handling features. In particular, the dashed line corresponds to a quite sporting car behaviour while the dotted course is related to more quiet vehicle cornering characteristics.
In the linear tract of the steering diagram, the uncontrolled car behaviour can be expressed as:

$$\frac{\delta}{\tau} = \left(\frac{l}{v^2} + K_V\right) a_y = \left(\frac{l}{v} + K_V v\right) \dot{\psi} \tag{12}$$

Where τ is the steering wheel ratio of the uncontrolled vehicle. The quantity K_V is the vehicle *understeer gradient*, which is defined as (see [1]):

$$K_V = \frac{m}{l}\left(\frac{b}{c_f} - \frac{a}{c_r}\right) \tag{13}$$

Equation (13) is obtained considering the cornering stiffness for the overall front (rear) axle instead of the single front (rear) wheels. Since the perceived handling quality of a vehicle with a lower understeer gradient is higher, reference curves in the linear tract are chosen by replacing K_V in (12) with the *desired* understeer gradient K_C such

that $0 < K_C < K_V$:

$$\frac{\delta}{\tau} = \left(\frac{l}{v^2} + K_C\right) a_{y,\mathrm{ref}} = \left(\frac{l}{v} + K_C v\right) \dot{\psi}_{\mathrm{ref}}, \quad \text{for } 0 \leq v\dot{\psi}_{\mathrm{ref}} \leq a_{y,l} \tag{14}$$

The lateral acceleration value $a_{y,l}$ is a design parameter which limits the linear tract of the controlled vehicle reference behaviour. Starting from this value, the desired yaw rate values are computed considering the following logarithmic relationship:

$$\begin{aligned} \frac{\delta}{\tau} &= \frac{\delta_{l,v}}{\tau} - \left(\frac{l}{v^2} + K_c\right)(\bar{a_y} - a_{y,l}) \ln\left(\frac{\bar{a_y} - a_{y,\mathrm{ref}}}{\bar{a_y} - a_{y,l}}\right) \\ &= \frac{\delta_{l,v}}{\tau} - \left(\frac{l}{v^2} + K_c\right)(\bar{a_y} - a_{y,l}) \ln\left(\frac{\bar{a_y} - v\dot{\psi}_{\mathrm{ref}}}{\bar{a_y} - a_{y,l}}\right), \quad \text{for } a_{y,l} < v\dot{\psi}_{\mathrm{ref}} < \bar{a_y} \end{aligned} \tag{15}$$

where $\delta_{l,v}$ is the handwheel angle value which corresponds to lateral acceleration $a_{y,l}$ at each vehicle speed value v. Equation (15) realizes a smooth connection between the linear tract of the curve and the chosen maximum lateral acceleration value $\bar{a_y}$. The latter is selected as the maximum lateral acceleration that can be reached as shown in Figure 5 (dashed line), without violating the physical upper bound suggested by [1]:

$$\bar{a_y} \leq 0.85\mu g \tag{16}$$

where μ is the available tyre-road friction and g is the gravity acceleration. Thus, a reference steering diagram as showed in Figure 5 is computed for each speed value v, so a map of values of $\dot{\psi}_{\mathrm{ref}}(\delta, v)$ is obtained. Figure 6 shows an example of such a static reference map. For negative values of δ, the symmetric map with respect to the one obtained for positive δ values is considered. The third step corresponds to the choice of the reference sideslip angle

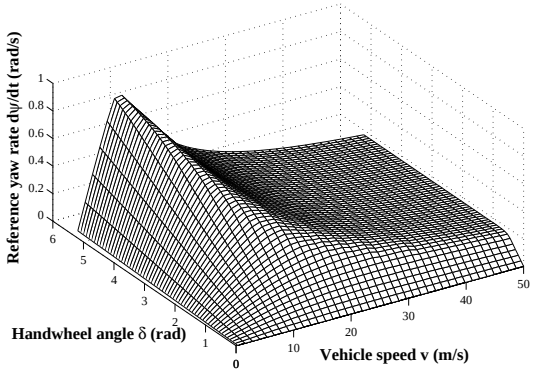

Figure 6. An example of yaw rate reference static map.

values $\beta_{\mathrm{ref}}(\delta, v)$. Since the objective is to limit the sideslip angle value during any maneuver, $\beta_{\mathrm{ref}}(\delta, v)$ is chosen, for each value of δ and v, as the lowest value of β that can be obtained given the corresponding reference yaw rate value $\dot{\psi}_{\mathrm{ref}}(\delta, v)$ and the saturation limits of the actuators. Note that the proposed strategy for the computation of the reference map $\mathcal{M}(\delta, v)$ can be iterated in order to obtain other specific objectives: for example, it is possible to re-calculate the yaw rate reference values in order limit the maximum sideslip angle that the vehicle is expected to reach in steady state maneuvers, if the values of $\beta_{\mathrm{ref}}(\delta, v)$ obtained at the end of the first iteration of the procedure are not satisfactory.

4.2 *IMC controller design*

Internal Model Control (IMC) techniques (see [12]) based on H_∞ optimization are able to satisfy robust stability requirements in presence of input saturation (see e.g. [14]). The basic IMC structure is reported in Figure 7.

However, as discussed in [13], IMC control may deteriorate the system performances in presence of actuator

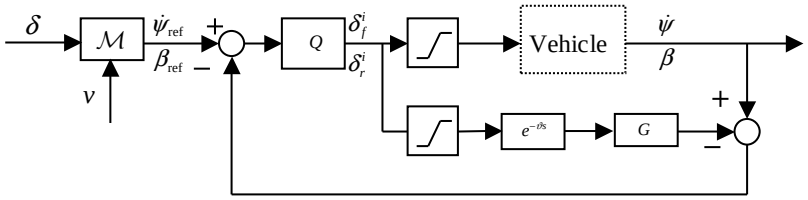

Figure 7. IMC scheme with saturating input.

saturation even in absence of model uncertainty. In order to improve the performances under saturation an enhanced robust IMC structure based on the anti-windup IMC solutions presented in [13, 22] has been proposed in [14]. The control scheme considered in [14] gives rise to a nonlinear controller made up by the cascade connection of a linear filter $Q_1(s)$ and a non linear loop Q_2 which replaces the linear controller $Q(s)$ as shown in Figure 8.

In linear operating conditions (i.e. when the saturation is not active) the improved IMC structure is equivalent to a

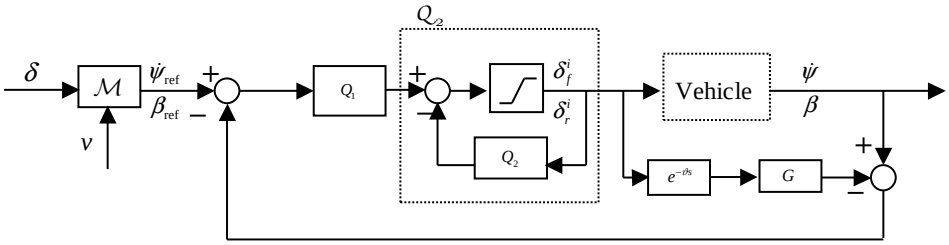

Figure 8. The proposed control scheme.

"standard" IMC controller of the form:

$$Q(s) = (I + Q_2(s))^{-1} Q_1(s) \tag{17}$$

The design procedure can be summarized in the following steps:

(i) A preliminary robust IMC controller $Q(s)$ is computed solving the following optimization problem:

$$\begin{aligned} Q(s) = \arg\min & \left\| W_S^{-1}(s)(I - G(s)Q(s)) \right\|_\infty \\ \text{s.t. } & \left\| \bar{\Gamma}(s)G(s)Q(s) \right\|_\infty < 1 \end{aligned} \tag{18}$$

where $\bar{\Gamma}(s)$ is a suitable real rational function, stable, whose magnitude strictly overbounds the frequency course $\Gamma(\omega)$ (see (6)) and the weight $W_S(s)$ takes into account a desired frequency response specification on the sensitivity function $S(s) = (I - G(s)Q(s))$

(ii) Using controller $Q(s)$ computed in the previous step, a controller $Q_2(s)$, via the design of a preliminary filter $\bar{Q}_1(s)$, is obtained according to the criteria introduced in [13, 22]. Note that $Q_2(s)$ must ensure the stability of the non linear loop Q_2 (see Figure 8). To this end, an upper bound γ_{Q_2} on the H_∞ norm of Q_2 has to be computed (see [14] for details). If γ_{Q_2} is finite then the stability of Q_2 is guaranteed. In case that the stability of Q_2 is not assured then a new controller design has to be performed starting from point (i), e.g. by relaxing the sensitivity requirements

(iii) Then, the linear controller $Q_1(s)$ can be designed by means of the following H_∞ optimization problem:

$$\begin{aligned} Q_1(s) = \arg\min & \left\| W_S^{-1}(s)\,(I - G(s)(I + Q_2(s))^{-1} Q_1(s)) \right\|_\infty \\ \text{s.t. } & \left\| \Gamma(s)G(s)\gamma_{Q_2}Q_1(s) \right\|_\infty < 1 \end{aligned} \tag{19}$$

Remark **Though the synthesis procedure employs an anti-windup scheme, it cannot be configured as a classical anti-windup design. In fact, the anti-windup design aims to modify the structure of an existing controller**

to improve performances in saturation conditions but leaving unmodified its behaviour in linear working situation. However, the design procedure employed in this paper may introduce modification in the "original" IMC controller $Q(s)$ (see [14]), thus changing the closed loop behaviour. In particular, comparing the robust stability condition $\|\bar{\Gamma}(s)G(s)Q(s)\|_\infty = \|\bar{\Gamma}(s)G(s)(I+Q_2(s))^{-1}Q_1(s)\|_\infty < 1$ in (18) with the one in (19), namely $\|\bar{\Gamma}(s)G(s)\gamma_{Q_2}Q_1(s)\|_\infty < 1$, it follows that $\|\bar{\Gamma}(s)G(s)(I+Q_2(s))^{-1}Q_1(s)\|_\infty \leq \|\bar{\Gamma}(s)G(s)\gamma_{Q_2}Q_1(s)\|_\infty$, since in general holds $\|(I+Q_2(s))^{-1}\|_\infty \leq \|\gamma_{Q_2}\|_\infty$. Therefore, more restrictive robust stability conditions are required by (19) with respect to (18). This may cause a worsening on the obtained sensitivity performances. Further comments about this point will be given in Section 5. .

5 Simulation results

The control design has been performed using transfer matrices $G_{\delta_{f,r}}(s)$ and $G_a(s)$ defined in (2) and (3) computed at a nominal speed $v = 100\,\text{km/h} = 27.7\,\text{m/s}$ and with the following values of the other involved parameters:

$m = 1798\,\text{kg}$	$J_z = 2900\,\text{kgm}^2$	$a = 1.13\,\text{m}$	$b = 1.57\,\text{m}$	$l_f = 0.3\,\text{m}$
$l_r = 0.3\,\text{m}$	$c_f = 76515\,\text{Nm/rad}$	$c_r = 96540\,\text{Nm/rad}$	$\vartheta = 20\,\text{ms}$	$K_f = 1$
$K_r = 1$	$\zeta_f = 0.306$	$\zeta_r = 0.306$	$\omega_f = 83.33\,\text{rad/s}$	$\omega_r = 139\,\text{rad/s}$

The saturation values for the control inputs δ_f^i and δ_r^i are $|\delta_f^i| \leq 30^\circ$, $|\delta_r^i| \leq 5^\circ$.
As to the feedback controller design, the desired performance weight to be used in the optimization problems (18) and (19) is described by the function:

$$W_S^{-1}(s) = 1.5\,\frac{s}{s+20}$$

Figure 9 (dotted lines) shows the frequency courses of the maximum singular value $\bar{\sigma}(\Delta(s))$ of the uncertainty $\Delta(s)$ (6), obtained by gridding over the parameter variations considered in Section 3. The overbound $|\bar{\Gamma}(j\omega)|$ is reported too (solid line). The function $\bar{\Gamma}(s)$ has to be chosen such that its magnitude overbounds the worst case course of $\bar{\sigma}(\Delta(s))$ obtained by the gridding procedure.

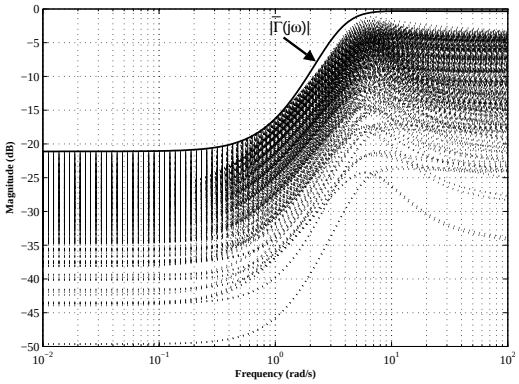

Figure 9. **Model set $\mathcal{G}$: maximum singular value $\bar{\sigma}(\Delta(j\omega))$ of the multiplicative output uncertainty (dotted) obtained with 500 perturbed plants and magnitude of the weighting function $\Gamma(s)$ (solid).**

To show in a realistic way the performances obtained by the proposed 4WS control approach, the controller has been discretized with a sampling time equal to 10 ms and simulations have been performed using a detailed nonlinear 14 degrees of freedom Simulink® model **([23]) of an Alfa Romeo 166 prototype**, validated on the basis of real vehicle measurements. In particular, the model degrees of freedom correspond to the standard three chassis translations and yaw, pitch and roll angles and the four wheel angular speeds and steering angles. Nonlinear characteristics obtained on the basis of measurements on the real vehicle have been employed to model the tyre, steer and suspension behaviour. Figure 10 shows the comparison between the model outputs and real measurements collected on an uncontrolled vehicle regarding a step steer maneuver with power off.

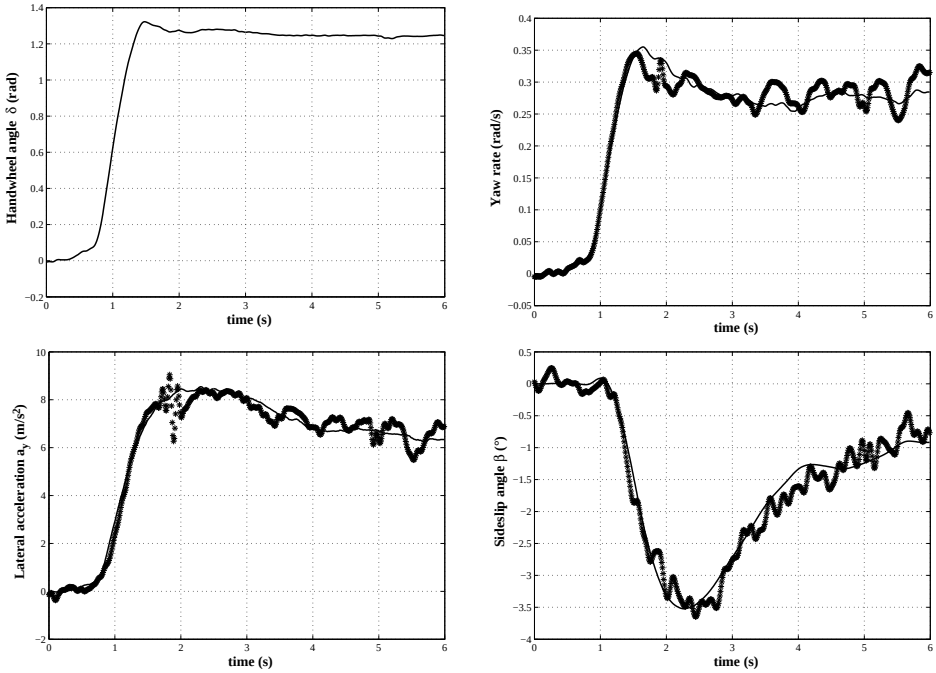

Figure 10. Comparison of simulated and real acquired vehicle data during a step steer maneuver with power off. Initial speed: 110 km/h. Upper left: handwheel input. Comparison between the values obtained with the 14 d.o.f. model (solid line) and collected experimental data (asterisks) for yaw rate (upper right), lateral acceleration (lower left), sideslip angle (lower right).

The following open loop (i.e. without driver's feedback) maneuvers have been chosen to test the controlled car safety, as well as steady state and transient handling performances, and to compare these characteristics with the uncontrolled vehicle ones:

- constant speed steering pad performed at 90 km/h: to evaluate steady state vehicle performances, handwheel angle is slowly increased (i.e. $5^\circ/\mathrm{s}$) while the vehicle is moving at constant speed, until the vehicle lateral acceleration limit is reached;
- steer reversal test with handwheel angle of 50° performed at 100 km/h, with a handwheel speed of $400^\circ/\mathrm{s}$. This test aims to evaluate the controlled car transient response performances: in Figure 11.(a) the employed handwheel angle behaviour is showed. To try out the control system robustness, the same test has also been performed with a tyre-road friction coefficient μ equal to 0.7 (wet road);
- handwheel step input of 30° performed at 80 km/h, with a handwheel speed of $400^\circ/\mathrm{s}$, and lateral wind disturbance during the cornering, with 100 km/h wind speed. The wind disturbance occurs after the transient of the reference step input is completed. In this test, vehicle mass was increased by 15%, with consequently changed inertial and geometrical vehicle characteristics. The purpose of this test is to evaluate the control system robustness in presence of disturbances and parameter variations.
- handwheel step input of 50° performed at 100 km/h, with a handwheel speed of $400^\circ/\mathrm{s}$, and a sudden loss of road friction ($\mu = 0.2$) at the left wheels between 1.3 s and 1.7 s. The purpose of this test is to evaluate the control system robustness in presence of differential left-right friction changes, simulating e.g. ice patches on the road.

Moreover, to test the effectiveness of the proposed approach also with driver's action, the following closed loop maneuver has been considered too:

- ISO double lane change maneuver as reported in [24], with constant test speed $v_{\mathrm{ref}} = 100\,\mathrm{km/h}$. The reference vehicle path in terms of yaw angle $\psi_{\mathrm{ref}}(t)$ is reported in Figure 11.(b). The lane change maneuver has been performed in nominal conditions and with vehicle mass increased by 25% (full load), with consequent geometrical and inertial parameters changes. The following driver's model has been used (see [24]):

$$\delta(s) = \frac{K_d}{\tau_d\, s + 1}\left(\psi_{\mathrm{ref}}(s) - \psi(s)\right)$$

Indeed, more complex driver models could be employed, which consider also the vehicle path deviation with respect to the reference (see e.g. [24]). However, the purpose of the considered closed loop maneuvers is to simply make a comparison between the handling properties of the uncontrolled vehicle and the controlled one, given the same driver model. As regards the values of the driver gain K_d and of the driver time constant τ_d, the following cases have been considered:

$$\begin{aligned} &\text{Driver 1: } K_d = 19.2,\ \tau_d = 0.25\,\text{s} \\ &\text{Driver 2: } K_d = 9.6,\ \tau_d = 0.15\,\text{s} \\ &\text{Driver 3: } K_d = 7.7,\ \tau_d = 0.08\,\text{s} \end{aligned}$$

Note that the values of τ_d range from 0.08 s (experienced driver) to 0.25 s (unexperienced driver), while the higher is the driver gain, the more aggressive is the driving action which could cause more likely vehicle instability.

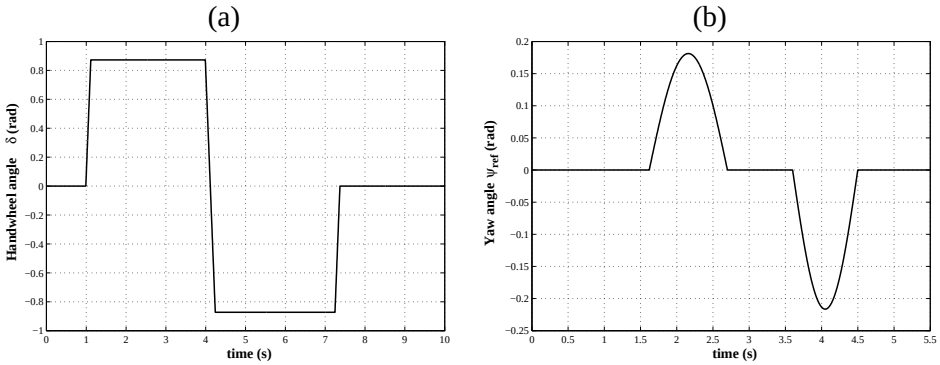

Figure 11. (a) Handwheel angle input for the steer reversal test. (b) Reference yaw angle $\psi(t)$ for the ISO double lane change test at 100 km/h

In Figure 12 the steering diagram and sideslip angle performance improvement is showed for the considered steering pad maneuver. The reference steering diagram and the one obtained with the controlled vehicle are superimposed, therefore the target vehicle behaviour, characterized by a lower understeer gradient, is reached while the vehicle sideslip angle value is kept close to zero. Note that the speed at which the maneuver has been performed is different from the nominal speed, thus showing control system robustness.

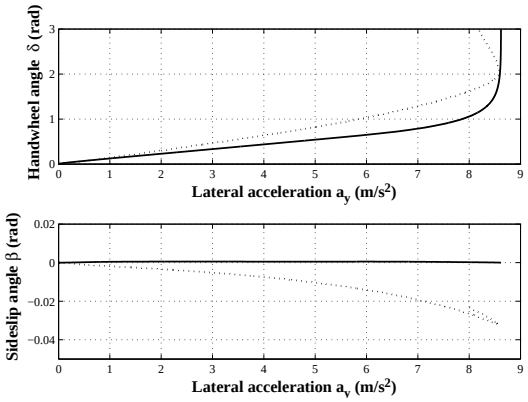

Figure 12. Comparison between the reference steering diagram (thin solid line) for steering pad maneuver at 90 km/h and the ones obtained for the uncontrolled vehicle (dotted) and for the controlled vehicle (solid). In the lower plot, sideslip angle behaviour is reported for the uncontrolled vehicle (dotted line) and for the controlled one (solid line)

The 50° steer reversal tests at 100 km/h allow to study the results obtained when the controlled vehicle reaches the yaw rate value of about 0.3 rad/s (see Figure 13), which corresponds to the lateral acceleration limit of about 8 m/s^2. The yaw rate response reported in Figure 13 shows the significant improvements of the system damping properties; at the same time the sideslip angle β is kept quite close to zero. Moreover, it can be observed that, according

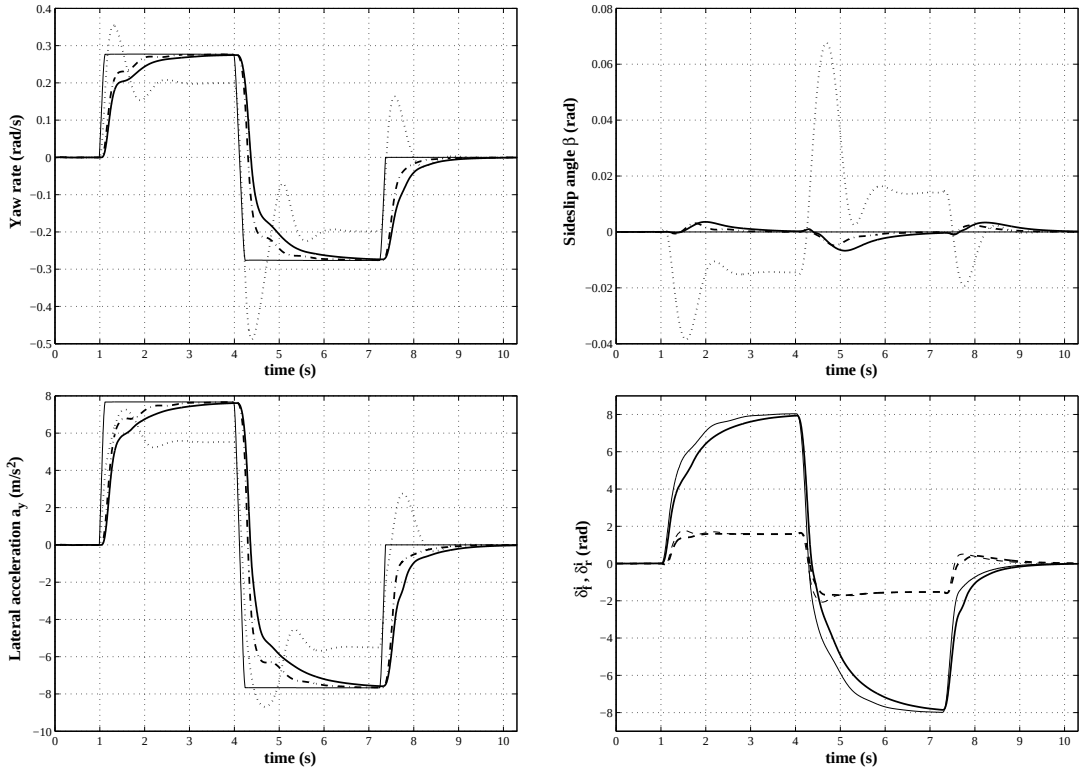

Figure 13. Steer reversal test at 100 km/h. Comparison between the reference (thin solid line), uncontrolled (dotted), controlled with anti-windup scheme (solid) and controlled without anti-windup scheme (dash-dot) vehicle yaw rate (upper left), sideslip angle (upper right) and lateral acceleration (lower left). Lower right: front (solid line) and rear (dashed line) steering angles for the controlled vehicle with anti-windup scheme (thick lines) and without anti-windup scheme (thin lines).

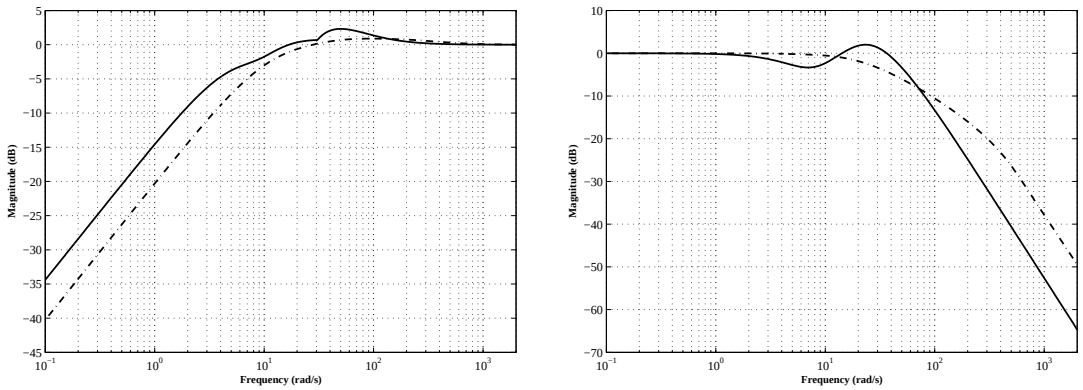

Figure 14. Comparison between the maximum singular values of the nominal sensitivity and complementary sensitivity functions. Left: $S_1(s)$ (dash-dot) and $S_2(s)$ (solid). Right: $T_1(s)$ (dash-dot) and $T_2(s)$ (solid)

to the chosen target steering diagram (see Figure 1.(a), solid line), the controlled vehicle reaches a higher lateral acceleration value. **In Figure 13 the behaviour of the controlled vehicle with the standard IMC controller $Q(s)$ obtained using (18) is reported too. Note that a slight increase of the settling time occurs when the controller obtained with (19) is used in absence of saturation. To better understand this point, in Figure 14 the maximum singular values of the nominal sensitivity $S_1(s) = (I - G(s)Q(s))$ and $S_2(s) = (I - G(s)(I + Q_2(s))^{-1}Q_1(s))$ and complementary sensitivity functions $T_1(s) = I - S_1(s)$ and $T_2(s) = I - S_2(s)$ obtained with (18) and (19) respectively are reported. Note the bandwidth reduction and the greater values of the resonance peaks, which illustrate in a quantitative way the performance degradation discussed in Section 4.2**. On the contrary, in presence of saturating input the classical IMC scheme shows much worse performances with respect to the enhanced IMC controller, as discussed later and shown in Figure 17, where a handwheel step plus friction loss maneuver is considered.

The results of the same test (i.e. 50° steer reversal at 100 km/h) with low friction coefficient are reported in Figure 15.

Note that, since no road friction variation was considered in model uncertainty evaluation, this test represents a very demanding robustness check. The control system is not able to reach the reference yaw rate and lateral acceleration values because of the insufficient friction between the tyres and the ground, since the reference maps have been generated supposing a friction coefficient equal to 1 (dry road). Anyway, the controlled vehicle is able to reach a higher yaw rate value with respect to the uncontrolled one, and the maximum controlled vehicle sideslip angle value $|\beta(t)|$ obtained during the test is equal to 0.02 rad, while the uncontrolled car reaches a peak of $|\beta(t)| = 0.09$ rad. Sideslip angle is therefore reduced, enhancing vehicle stability properties.

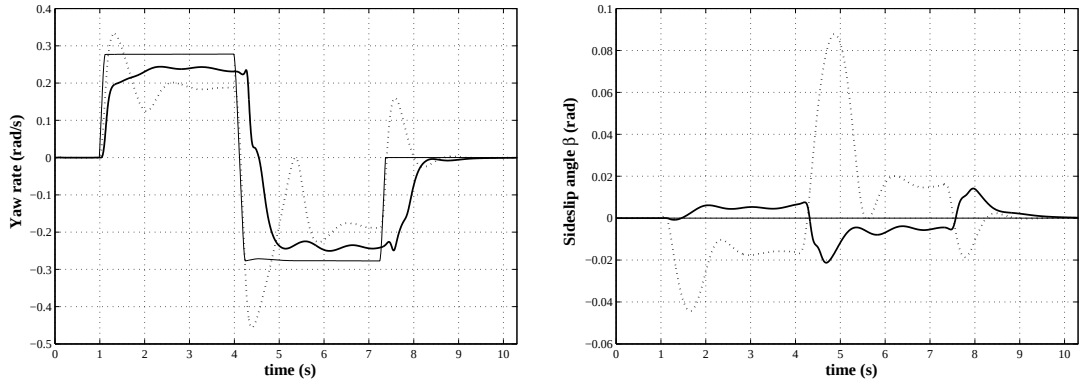

Figure 15. Steer reversal test at 100 km/h, wet road. Handwheel value: 50°. Comparison between the reference (thin solid line), uncontrolled (dotted) and controlled (solid) vehicle yaw rate (left) and sideslip angle (right).

The results reported in Figure 16 related to the handwheel step with lateral wind disturbance test, with increased vehicle mass, show the control system capability to reject disturbances and to keep stability in presence of parameter variations.

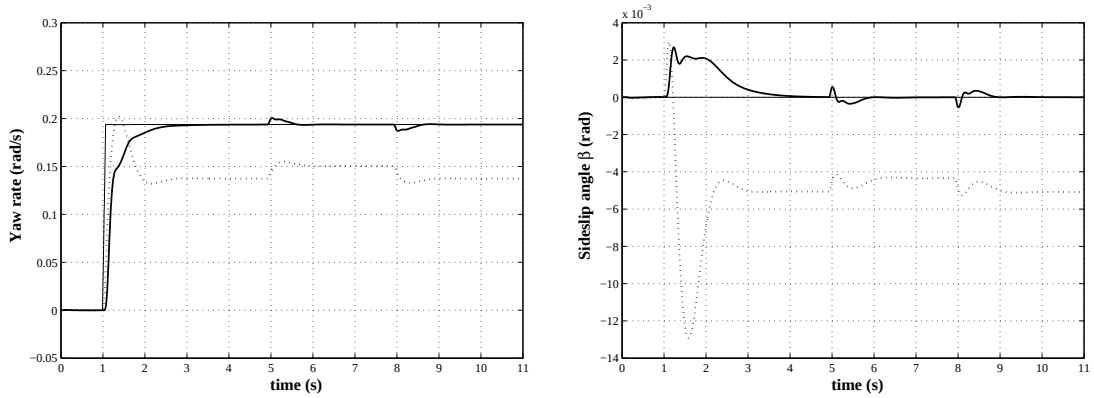

Figure 16. Handwheel step input of 30° at 80 km/h, with vehicle mass increased by 15%, plus 100 km/h wind disturbance between 5s and 8s. Comparison between the reference (thin solid line), uncontrolled (dotted) and controlled (solid) vehicle yaw rate (left) and sideslip angle (right).

Figure 17 shows the results of the handwheel step test in presence of a sudden loss of available friction at the left wheels: vehicle stability is kept, with lower sideslip angle, and control system is able to handle effectively the saturation of the rear steering angle. In particular, it is shown how the employed enhanced IMC structure avoids performance degradation which occurs when no anti-windup structure is employed (see Figure 7). The uncontrolled and controlled vehicle paths are also reported, showing the enhanced manoeuvrability of the latter.

The ISO double lane change at 100 km/h with nominal and increased vehicle mass allows to evaluate the controlled vehicle handling and safety improvement, employing three different simple driver models. The uncontrolled car led by Driver 1 is not stable both in the nominal case and with increased vehicle mass, while the controlled car is able to achieve stability and quite good overall performances (see Figure 18 for the nominal case). With Driver model 2 the uncontrolled nominal vehicle stability is kept, but the driver's action on the handwheel angle δ causes an underdamped sideslip angle behaviour. The results of the same test with increased vehicle mass are reported in Figure 20. In this case, instability occurs in the final part of the maneuver with the uncontrolled vehicle (as it can be noted in Figure 21, which shows a typical example of unstable vehicle trajectory), while the controlled car

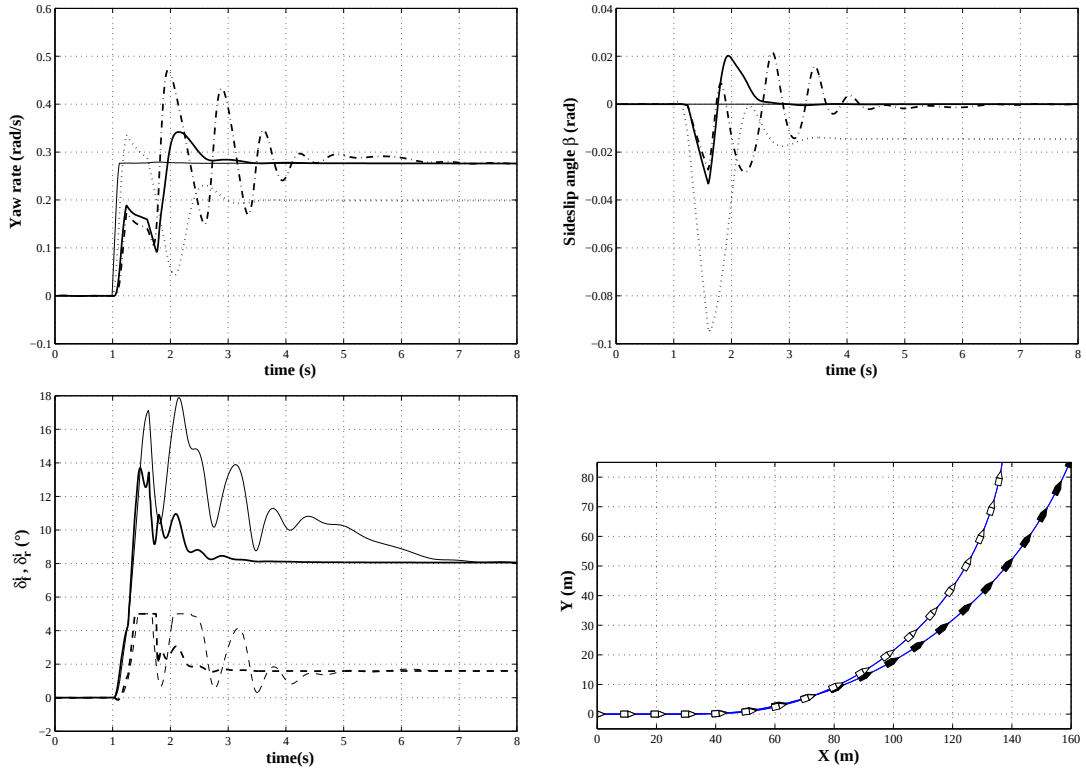

Figure 17. Handwheel step input of 50° at 100 km/h, with friction loss at the left wheels between 1.3 s and 1.6 s. Comparison between the reference (thin solid line), uncontrolled (dotted), controlled with anti-windup scheme (solid) and controlled without anti-windup scheme (dash-dot) vehicle yaw rate (upper left) and sideslip angle (upper right). Lower left: front (solid line) and rear (dashed line) steering angles for the controlled vehicle with anti-windup scheme (thick lines) and without anti-windup scheme (thin lines). Lower right: uncontrolled (black) and controlled with anti-windup scheme (white) vehicle paths.

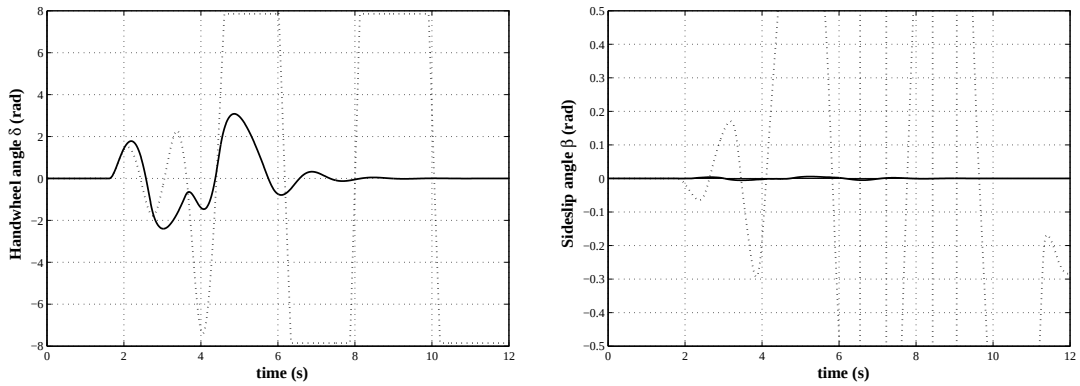

Figure 18. ISO double lane change at 100 km/h, nominal vehicle mass, Driver 1. Comparison between the uncontrolled (dotted) and controlled (solid) driver input (left) and vehicle sideslip angle (right).

still has a well damped response, with very low β values, which leads to less oscillating steering input and vehicle stability during the whole test. Finally, the results of the same test performed with Driver model 3 (see Figure 22 for the case of increased vehicle mass) show how the achieved handling improvements are less evident. However, the handwheel input in the controlled case is still less oscillating and sideslip angle is much lower than the uncontrolled case.

6 Conclusions

A vehicle equipped with a four wheel steer by wire system has been considered and a robust non parametric control approach using both vehicle yaw rate and sideslip angle feedbacks has been introduced. Reference yaw rate and sideslip angle, which enhance the vehicle handling and stability properties, are computed on the basis of the vehicle

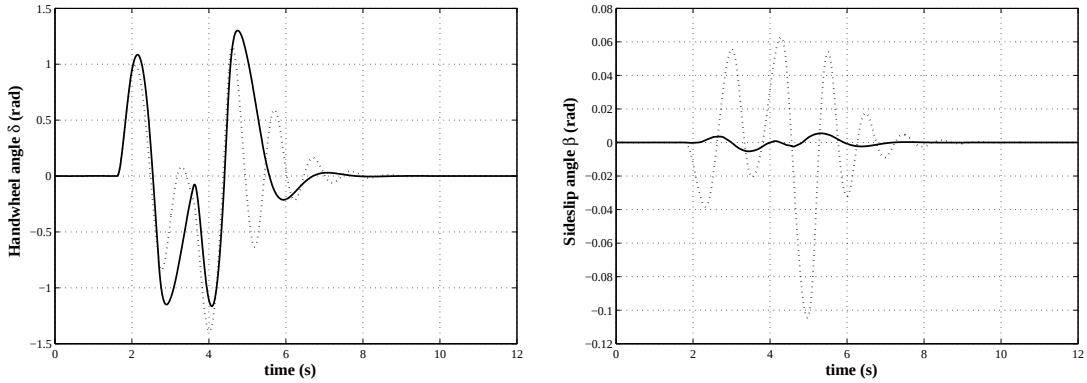

Figure 19. ISO double lane change at 100 km/h, nominal vehicle mass, Driver 2. Comparison between the uncontrolled (dotted) and controlled (solid) driver input (left) and vehicle sideslip angle (right).

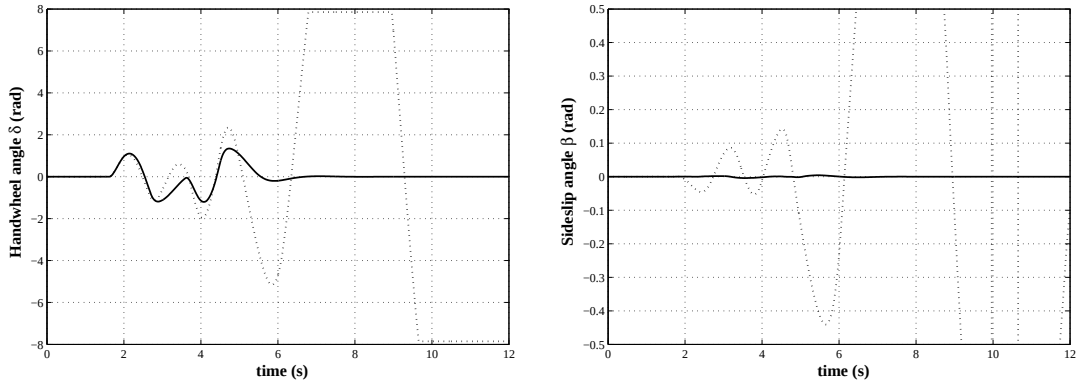

Figure 20. ISO double lane change at 100 km/h, vehicle mass increased by 25% with consequent inertial and geometrical parameters changes, Driver 2. Comparison between the uncontrolled (dotted) and controlled (solid) driver input (left) and vehicle sideslip angle (right).

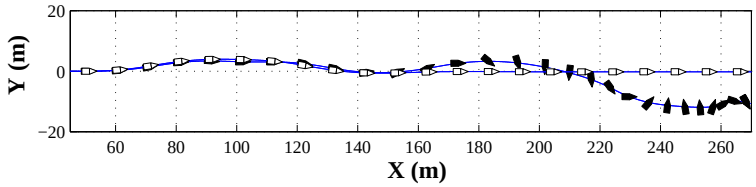

Figure 21. ISO double lane change at 100 km/h, vehicle mass increased by 25% with consequent inertial and geometrical parameters changes, Driver 2. Comparison between the uncontrolled (black) and controlled (white) vehicle paths.

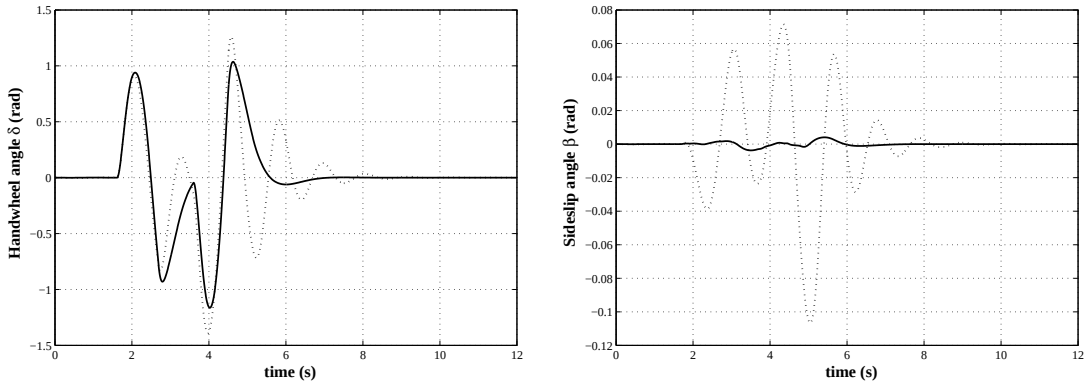

Figure 22. ISO double lane change at 100 km/h, vehicle mass increased by 25% with consequent inertial and geometrical parameters changes, Driver 3. Comparison between the uncontrolled (dotted) and controlled (solid) driver input (left) and vehicle sideslip angle (right).

speed and of the handwheel angle imposed by the driver. The proposed control structure exploits the features of Internal Model Control strategies which allow both to guarantee robust stability and to enhance performances in presence of input saturation. Actuator dynamics are taken into account in control system design.

Simulation results performed on an accurate model of the considered vehicle demonstrate the effectiveness of the proposed control structure. In particular, it has been shown that the achieved performances are very close to the target understeer objectives, a highly damped behaviour in impulsive open loop maneuvers has been obtained, stability is guaranteed in presence of lower tyre-road friction and vehicle handling and stability properties are significantly improved in presence of driver's action.

References

[1] Rajamani, R., 2005, *Vehicle Dynamics and Control* (New York: Springer).
[2] V. Zanten, A. T., 2000, Bosch ESP systems: 5 years of experience.*SAE Technical Paper No. 2000-01-1633*.
[3] Furukawa, Y., Yukara, N., Sano S., Takeda, H. and Matsushita, Y., 1989, A review of four wheel steering studies from the viewpoint of vehicle dynamics and control. *Vehicle System Dynamics*, **18**, 151–186.
[4] Hirano, Y. and Fukatani, K., 1996, Development of robust active rear steering control. Paper presented at 3rd International Symposium on Advanced Vehicle Control, Aachen, Germany, 24–28 June.
[5] Ackermann, J., 1994, Robust decoupling, ideal steering dynamics and yaw stabilization of 4ws cars. *Automatica*, **30**, 1761–1768.
[6] Vilaplana, M. A., Mason, O., Leith, D. J. and Leithead,W. E., 2005, Control of yaw rate and sideslip in 4-wheel steering cars with actuator constraints. *Lecture Notes in Computer Science*, **3355**, 201–222.
[7] Malan, S., Taragna, M., Borodani, P. and Gortan, L., 1994, Robust performance design for a car steering device. Paper presented at 33rd IEEE Conference on Decision and Control, Lake Buena Vista, USA, 15–17 December.
[8] Ackermann, J., Guldner, J., Steinhausner, R. and Utkin, V. I., 1995, Linear and nonlinear design for robust automatic steering. *IEEE Trans. on Control System Technology*,**3**, 132–143.
[9] Güvenç, B. A., Bünte T. and Güvenç, L., 2004, Robust two degree-of-freedom vehicle steering controller design. *IEEE Trans. on Control System Technology*, **12**, 627–636.
[10] Gerhard, J., Laiou, M.-C., Mönnigmann M., Marquardt, W., Lakehal-Ayat, M. and Busch, E. A. R., 2005, Robust yaw control design with active differential and active roll control systems. Paper presented at 16th IFAC World Congress, Prague, Czech Republic, 3–8 July.
[11] Canale, M., Fagiano, L., Milanese, M. and Borodani, P., 2007, Robust vehicle yaw control using an active differential and IMC techniques. *Control Engineering Practice*, **15**, 923–941.
[12] Morari, M. and Zafiriou, E., 1989, *Robust Process Control* (Englewood Cliffs, NJ:Prentice Hall).
[13] Zheng, A., Kothare, M. and Morari, M., 1994, Anti-windup design for internal model control. *International Journal of Control*, **60**, 1015–1022.
[14] Canale, M., 2004, Robust control from data in presence of input saturation. *International Journal of Robust and Nonlinear Control*, **14**, 983–998.
[15] Ryu, J. and Gerdes, J. C., 2004, Integrating inertial sensors with gps for vehicle dynamics control. *Journal of Dynamic System, Measurements and Control*, **126**, 243–254.
[16] Piyabongkarn, D., Rajamani, R., Grogg, J. A. and LewJ. Y., 2006, Development and experimental evaluation of a slip angle estimator for vehicle stability control. Paper presented at 25th American Control Conference, Minneapolis, USA, 14–16 June.
[17] Fittanto, D. A. and Senalik, A., 2004, Passenger Vehicle Steady-State Directional Stability Analysis Utilizing EDVSM and SIMON. Paper presented at 2004 HVE Forum, San Francisco, USA, 3–7 May.
[18] Data S. and Frigerio, F., 2002, Objective evaluation of handling quality. *Journal of Automobile Engineering*, **216**, 297–305.
[19] Vilaplana M. A. and Mason, O. and Leith, D. J. and Leithead, W. E., 2004, Control of Yaw Rate and Sideslip in 4–Wheel Steering Cars with Actuator Constraints. *Journal of passenger car: mechanical systems*, **113**, 1082–1094.
[20] Skogestad S. and Postlethwaite, I., 2005, *Multivariable Feedback Control*(UK:Wiley).
[21] Bakker, E., Lidner, L. and Pacejka, H., 1989, A new tyre model with an application in vehicle dynamics studies. *SAE Paper 890087*.
[22] Goodwin, G., Graebe, S. and Levine, W., 1993, Internal model control of linear systems with saturating actuators. Paper presented at 2nd European Control Conference, Gröningen, Netherlands, 28 June-1 July.
[23] Reckziegel, G., 2004, Active control systems for stability of 4WS vehicles, Master Thesis (in italian), Politecnico di Torino, Italy, December 2004.
[24] Genta, G., 2003, *Motor Vehicle Dynamics, II ed.* (World Scientific)